Edge electrospinning for high throughput production of quality nanofibers

View the article online for updates and enhancements.

Edge electrospinning for high throughput production of quality nanofibers

N M Thoppey[1], J R Bochinski[2], L I Clarke[2] and R E Gorga[1]

[1] Fiber and Polymer Science Program, NC State University, Raleigh, NC 27695, USA
[2] Department of Physics, NC State University, Raleigh, NC 27695, USA

E-mail: liclarke@ncsu.edu and regorga@ncsu.edu

Abstract
A novel, simple geometry for high throughput electrospinning from a bowl edge is presented
that utilizes a vessel filled with a polymer solution and a concentric cylindrical collector.
Successful fiber formation is presented for two different polymer systems with differing
solution viscosity and solvent volatility. The process of jet initiation, resultant fiber morphology
and fiber production rate are discussed for this unconfined feed approach. Under high voltage
initiation, the jets spontaneously form directly on the fluid surface and rearrange along the
circumference of the bowl to provide approximately equal spacing between spinning sites.
Nanofibers currently produced from bowl electrospinning are identical in quality to those
fabricated by traditional needle electrospinning (TNE) with a demonstrated ~40 times increase
in the production rate for a single batch of solution due primarily to the presence of many
simultaneous jets. In the bowl electrospinning geometry, the electric field pattern and
subsequent effective feed rate are very similar to those parameters found under optimized TNE
experiments. Consequently, the electrospinning process per jet is directly analogous to that in
TNE and thereby results in the same quality of nanofibers.

S Online supplementary data available from stacks.iop.org/Nano/22/345301/mmedia

(Some figures in this article are in colour only in the electronic version)

1. Introduction

Electrospinning is a straightforward yet elegant technique [1–5] to manufacture nanofibers (i.e. fibers having a diameter ~100–1000 nm) using a wide range of polymer solutions or melts [6–11]. The resulting electrospun nanofibrous structures have useful properties, such as a high surface-to-volume ratios and large porosity values (~70%) [6]. The high porosity and micro-sized pores enable trapping of liquid and air-borne particles for very efficient air and liquid filtration applications [12]. Nanofibrous scaffolds fabricated from biocompatible and biodegradable polymers mimic natural extracellular matrices, which makes them suitable for tissue engineering [13–18] and other biomedical applications [19–21], including drug delivery [14, 22–25] and wound dressing [26]. Functionalized nanocomposites, such as nanofibers doped with metal oxides or carbon compounds, have been extensively studied for energy storage applications [22, 27–33]; moreover,

recent work has utilized the surface plasmon resonance of metallic nanoparticles embedded in fibers as a novel means to thermally process the material [34].

While traditional single-needle electrospinning (TNE) [6–11, 35, 36] is cost-effective, convenient and widely used in research settings, typical low production rates in the range of 0.01–0.1 g h^{-1} [37, 38] inhibit industrial implementation, which is crucial for emergent technological applications utilizing nanofibrous materials. Figure 1 shows a common TNE set-up consisting of a programmable precision syringe pump that expels polymer solution through a charged conducting needle. The polymer solution exiting the needle tip forms a jet which undertakes a linear path followed by a whipping region that elongates and dries the nanofiber before it is gathered onto the grounded collector. Material throughput in TNE can be improved by utilizing higher solution feed rates but a detrimental consequence is that the fibers produced under those processing conditions have larger
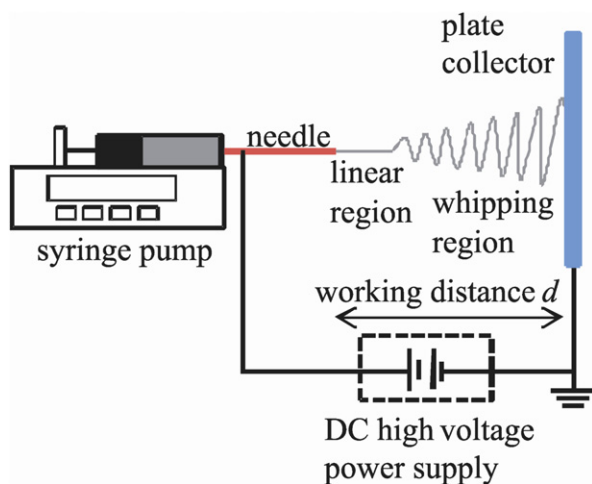
Figure 1. Schematic side view of a traditional needle electrospinning (TNE) apparatus, consisting of a precision syringe pump, a conducting needle charged by a positive polarity high voltage power supply and a flat, grounded collector.

diameters. The electrospinning process can be scaled up by forming many spinning sites [39] instead of the single site at the end of the needle tip in the traditional method. As discussed previously [40], one categorization scheme is to divide these scale-up approaches into two groups depending on whether the fluid flow at the spinning site is spatially restricted. Approaches that utilize an enclosure such as a needle [41–43], nozzle [44] or tube [37, 38] through which the polymer fluid is extruded are categorized as confined systems. Schemes under which the polymer fluid flows over the surface of another material [45] or if the electrospinning occurs directly from a fluid reservoir [46, 47] are referred to as unconfined systems. Generally, scale-up approaches using confined fluid systems produce high quality nanofibers (with small fiber diameters and a more homogeneous fiber diameter distribution) but are prone to clogging and often involve engineering complexity in the nozzle design. In the past, unconfined systems have resulted in fibers produced with both innately larger diameters and a broader distribution of diameter sizes [46]. We have recently demonstrated [40] that unconfined fluid streams from the edge of a charged plate could be utilized to electrospin nanofibers that are morphologically almost identical to those from TNE; moreover, by using multiple fluid streams many spinning sites could also potentially be formed. We argued that the high nanofiber quality resulted from an electric field magnitude and gradient at the edge of the plate (where spinning occurred) that was similar to that present near the needle tip in TNE. Thus, such edge-plate electrospinning established that high quality fibers could be facilely produced in a simple, unconfined system approach.

In this work, we extend these previous results by utilizing the lip of a bowl for electrospinning; analogously, this concept can be thought of as curving the plate edge into a cylindrical geometry (figure 2). The narrow edge of the bowl serves to produce a strong electric field magnitude and gradient which is similar to that at the single spinning site in TNE. Multiple jets are initiated spontaneously from the polymer fluid directly at
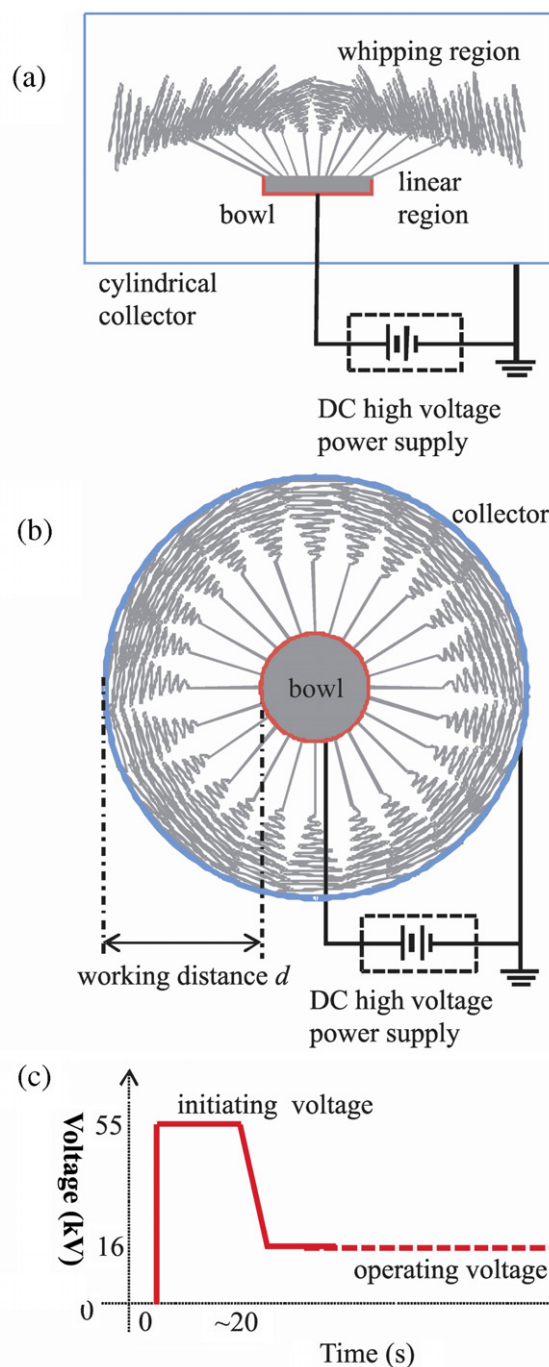
Figure 2. Schematic of the bowl electrospinning apparatus as viewed from (a) the side (cutaway) and (b) the top looking down, consisting of the fluid-filled bowl, a positive polarity high voltage power supply and a concentric, cylindrical grounded collector. (c) The timing sequence of the applied voltages: to initiate jets, the voltage is 55 kV for ∼20 s, then rapidly reduced to 16 kV and maintained at this level for stable operation.

the lip of the bowl, as well as further inside the bowl's interior which then migrate to the edge and organize to form relatively equally spaced spinning sites around the bowl circumference. Unlike in the edge-plate geometry, jets form and spinning occurs directly from the fluid surface within the bowl, rather than utilizing falling or elongated droplets; moreover, the bowl

itself serves as the source of the polymer solution instead of gravity-assisted fluid streams. An initial brief high voltage interval aids in forming the jets; subsequently, the voltage is reduced to a lower operating value for stable electrospinning and nanofiber formation. The resultant spinning sites produce high quality nanofibers which are gathered on a concentric, grounded cylindrical collector. The collected fibers exhibit properties (small average diameter and narrow diameter distribution) similar to those fabricated under optimal needle electrospinning (TNE) conditions. Furthermore, this approach avoids additional system complexity of moving parts present in other unconfined feed systems such as the rotating cylinder in the Nanospider™. Under the current design, where the bowl is filled once and does not possess a replenishing reservoir, the throughput of the electrospinning process is increased by 40 times over TNE, approximately corresponding to the average number of spinning sites present. We demonstrate that this simple bowl-spinning approach is applicable to a variety of polymers in aqueous and non-aqueous-based solvent systems and to polymer solutions having differing viscosities.

2. Experimental details

2.1. Materials

Polyethylene oxide (PEO) (polycaprolactone (PCL)) with an average molecular weight of $400\,000$ g mol^{-1} ($80\,000$ g mol^{-1}) was purchased from Scientific Polymer Products (Sigma Aldrich), and used without further purification. Solutions of 6 weight per cent (wt%) PEO in deionized water (12 wt% PCL in equal parts of dichloromethane (DCM) and dimethyl-formamide (DMF)) were stirred at room temperature for 24 h (3 h) to aid dissolution. Except when otherwise specified, PEO solutions were used in all experiments. In some experiments, PEO solutions were tinted with rhodamine 590 chloride (R6G) (Exciton) (0.001 wt%) in order to provide enhanced imaging contrast for viewing the jet initiation process and subsequent stabilized jets. Zero shear viscosity of the PEO (PCL) solution at 25 °C was determined to be 9250 cP (170 cP) using a rheometer (REOLOGICA Instruments AB, StressTech).

2.2. Apparatus

In TNE experiments (figure 1), the polymer solution was supplied through a 10 cm long stainless steel needle (gauge 20) using a 10 ml plastic syringe and programmable syringe pump (New Era Systems, Model No. NE-1000). The conductive needle (shaded red in figure 1) was electrically connected to a variable, positive polarity high voltage power supply (Glassman High Voltage, Model No. FC60R2). A 15.25 cm in diameter, aluminum collector plate (shaded blue in figure 1) was electrically connected to the ground potential and located a working distance d from the charged needle tip, centered on and oriented orthogonally to the needle's long axis. Optimized parameters for the production of nanofibers using TNE of PEO (PCL) were an applied voltage of 11 kV, a needle-to-collector working distance of 15 cm and a solution feed rate of 5 μl min^{-1} (55 μl min^{-1}).

In the scale-up electrospinning experiments (figures 2(a) and (b)), a premeasured volume of polymer solution was loaded into an aluminum vessel machined from a single piece of material to have 9 cm inside diameter, 0.03 cm wall thickness and 0.9 cm depth. We refer to this three-sided cylindrical enclosure as a 'bowl'; the bottom face of the bowl was electrically connected to the high voltage power supply to act as the source electrode, akin to the needle in the TNE set-up. A 1.27 cm diameter threaded hole at the bottom center of the bowl, normally sealed during the experiments with a translucent plastic plug, acted as a convenient drain port. An aluminum hollow thin cylindrical collector, 39 cm in diameter, 0.01 cm in thickness and 37 cm in height, was connected to the ground potential and placed concentrically to the bowl in order to obtain a 15 cm working distance (determined as the distance normal between the outer surface of the bowl and the inner surface of the collector). The cylindrical collector could be displaced vertically while the working distance remained fixed; at all times, the collector extended vertically at least ± 9 cm relative to the horizontal plane defined by the lip of the bowl, which we refer to as the 'bowl edge plane'. In both TNE and bowl electrospinning experiments, the collector surfaces that faced the source electrodes (needle or bowl) were covered with conductive aluminum foil in order to easily remove the electrospun mat samples for further measurements.

Bowl electrospinning experiments utilized two different high voltage power supply settings (figure 2(c)). First, in order to facilitate jet formation an 'initiating' high voltage setting was applied for a brief time interval. Then, the voltage was reduced to a lower 'operating' level where jets were quasi-stable but no longer spontaneously forming, and high quality fibers could be collected. During the jet initiation period, electrospraying or streaming events frequently occurred (i.e. wet solution was propelled directly to the collector); thus the cylindrical collector was first positioned so that the bowl edge plane was approximately centered on the lower half of the collector (i.e. with 28 cm above and 9 cm below the bowl edge plane) in order that any excess solution was deposited only on the lower half of the collector. After the rapid voltage reduction, the collector was also quickly manually lowered to a new position centered on the top half of the collector (now with 9 cm above and 28 cm below the bowl edge plane) so that fabricated nanofibers were preferentially deposited on the upper half of the inner collector surface. In this manner, the wet solution flowing under gravity could not dissolve the high quality nanofibers that were manufactured at a later time under the stable operating voltage. In order to optimize the jet initiation process, survey experiments with PEO were carried out with a range of fluid volumes (60–80 ml), initiation high voltages (35–55 kV), initiation time duration (10–25 s) and stable operating voltage (15–21 kV). The most favorable results were obtained for 78 ml with an initiation voltage of 55 kV applied for ∼20 s, before a manual reduction (over ∼2–3 s) to a stable operating voltage of 16 kV as the cylindrical collector was simultaneously lowered. For PCL, a fluid volume of 78 ml and an operating voltage of 30 kV were used; no initiating voltage interval was required (see section 3.2).

A camcorder (Sony, Model DCR-SR68) with an enhanced viewing lens (Zeiss, 6 mm × 18 mm T monocular) and a

digital single-lens reflex (SLR) camera (Olympus, Model E-620) recorded images of the electrospinning process while the polymer jets were continuously illuminated by a halogen lamp (Northern Industrial Lighting, Model 1002) and/or a light source comprised of a square array of white LEDs (Visual Instrumentation Corporation, Model 900445).

2.3. Fiber characterization

Nanofiber morphology was studied with a scanning electron microscope (SEM) (JEOL JSM-6400 FE) operating at 5.0 kV. The samples were sputter-coated (Technics Inc., Hummer II) with Au–Pd at a thickness of ∼100 Å to produce a conductive surface and reduce charging effects. The SEM images were analyzed using Revolution™ software to measure the fiber physical size characteristics; 25 individual measurements were made on each sample to determine the mean diameter and standard deviation.

Porosity of nanofibrous mats was characterized from the SEM images using Image J Analyzer software; the images were converted to grayscale and analyzed to identify the top layer of the mat and determine the number of filled (belonging to this first fiber layer) and unfilled pixels [34, 48–52]. In order to assess the overall quality of the electrospun mats from TNE and bowl electrospinning configurations, we define a parameter called spinnability [40] as the fraction of the mat which retained the fibrous morphology compared to areas which may be damaged due to the streaming events during jet initiation. The spinnability was measured by analysis of SEM images of characteristic portions of the mat. For an ideal, stable configuration, where no streaming or spraying events occur, spinnability will be maximal (i.e. 100%).

Nanofibrous material production rates were calculated by electrospinning for known time periods, measuring the resultant mat mass by comparing the weight of the aluminum foil before and after spinning, and then normalizing to obtain the fabrication rate in grams per hour (g h^{-1}).

2.4. Electric field simulations

The electric fields generated under the different electrospinning geometries and processing parameters were modeled using Maxwell 3D (ANSOFT Corporation). Maxwell 3D utilizes finite element methods and adaptive meshing to provide a converged solution. The experimental configurations (TNE, bowl electrospinning and edge-plate electrospinning) were simulated by defining to scale structures using the experimentally realized parameters (applied voltages, working distances, and source/collector dimensions and material composition). Typical optimized simulation parameters resulted in a minimum (maximum) mesh element dimension of <0.05 mm (0.13 mm) with a total ∼10^6 mesh volume elements, where 20–30% of the total were used to define the source electrode in order to provide high spatial resolution in the most experimentally interesting region.

## 3. Results and discussion

3.1. Electric field modeling

Two-dimensional planar slices of the full three-dimensional simulation taken through the center axis of symmetry for the TNE (top row) and bowl electrospinning (second row) configurations are shown in figure 3, with the associated color legends given on the left side. The spatial scales of the first two columns are identical; the third column is a 50× magnified view of the end of each source electrode. The first and third columns represent scalar plots where the colors illustrate the magnitude of the electric field in the plane; the second column depicts a vector plot to show field directions in the same region as the first column, where the arrow color indicates the magnitude of the electric field at that location.

The first column illustrates half of each source electrode, respectively, where the grounded collectors (not shown) are located 15 cm to the right side of each electrode. As depicted in the third column, the peak electric field amplitude for the bowl electrospinning under the initiating voltage is comparable to that for TNE under optimal processing conditions (∼1.6 × 10^7 V m^{-1}). For TNE, the vector plot (second column) demonstrates that the direction of the electric field where the jet forms at the center of the needle tip is oriented directly towards the collector (i.e. horizontal and pointing to the right in figure 3); moreover, the magnitude of the field at this location is reduced compared to the peak value, to ∼5 × 10^6 V m^{-1}. This result can be understood by considering the cylindrical symmetry of the needle and recognizing that the vertical field components cancel. In contrast, for the bowl electrospinning configuration, jet formation at the bowl edge occurs directly at the field maximum and is directed at a positive angle of ∼30° relative to the horizontal.

For completeness, we also compare the bowl electro-spinning configuration to a previously reported edge-plate spinning geometry (see supplementary information, available at stacks.iop.org/Nano/22/345301/mmedia) under stable operating conditions [40]. In both optimal fiber-producing spinning configurations, the peak electric field amplitudes are approximately the same (and similar to that of optimal TNE where the jet forms) and the field direction at this location corresponds to the observed jet orientation. We note that the field values given for the edge-plate geometry differ from those in the previous report; this is due to the higher accuracy from the full three-dimensional simulation and finer mesh size employed, and represents an improved modeling result.

3.2. Jet initiation

Figure 4 summarizes the process of jet formation when the initiating voltage is applied (in this case, from 1 to 17 s) for the relatively viscous 6 wt% PEO solution (9250 cP). Sequential images from the camcorder video are displayed, viewing the experiment from the top looking directly down, with illumination provided by the white LED light source located behind (above) the camera. The bowl is oriented concentrically to the cylindrical collector (not shown). Deformation of the fluid is observed almost immediately (left to right, top row),
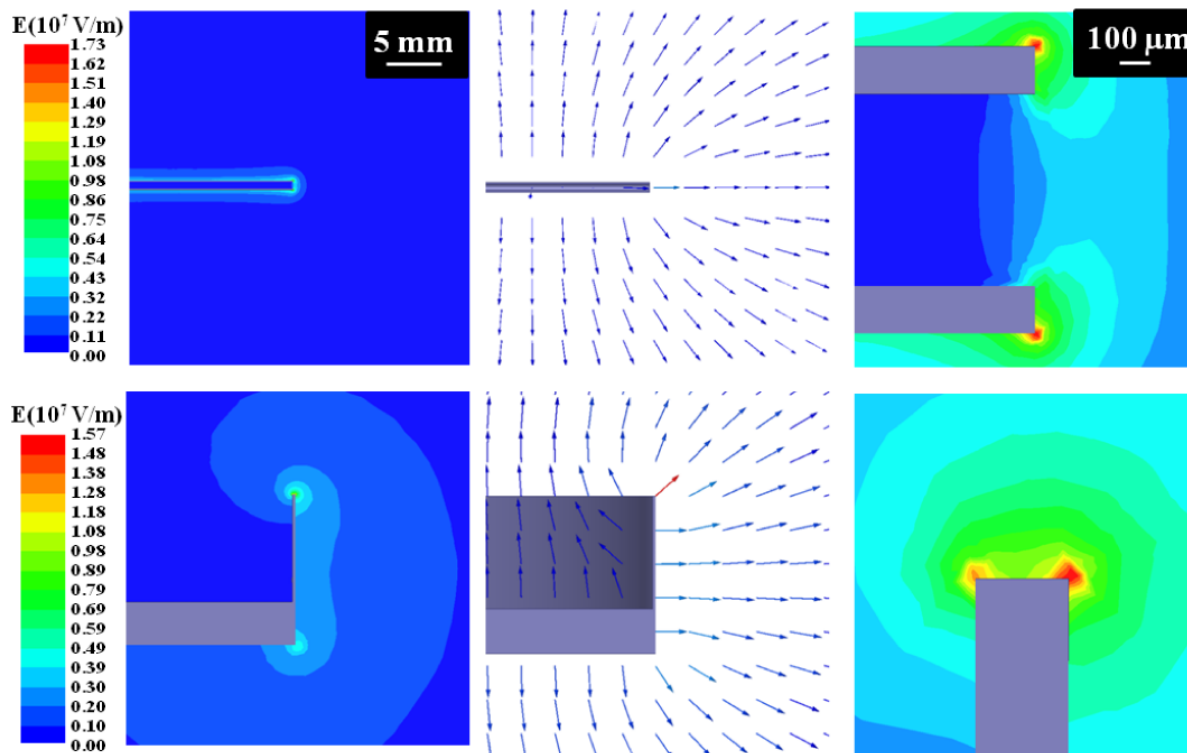
Figure 3. Simulations of the electric field distributions under processing parameters for optimal TNE at 15 cm and 11 kV (top row) and the jet initiation for bowl electrospinning at 15 cm and 55 kV (lower row). Color scale is given to the left of each row. Right column: 50× magnified image of the needle tip and bowl lip, respectively.

with sharp spatial instabilities developing rapidly over the first few seconds. After 4 s, these cone-like protrusions result in jet formation (5 s) and streaming of polymer solution directly to the collector (6–7 s).

For the remainder of the initiating period, jets at the bowl edge bifurcate, separate and reorganize, while fluid instabilities that form in the bowl interior migrate to the edge. After 17 s at the initiation voltage, the jets at the edge are relatively equally spaced and of similar magnitude. Due to the magnitude of the voltage applied during this initiating interval, the electric field is too large for good quality nanofiber formation from the free fluid surface and detrimental electrospraying or streaming events primarily occur. Thus, at this point in time, the voltage is reduced to the operating value. Quasi-stable jets, which produce the high quality nanofibers, are approximately symmetrically distributed around the edge of the bowl (see the 20 s image in figures 4 and 7); note, the cone-like protrusions disappear when the voltage is reduced. Under this single-batch process, some jets persist for up to 80 min (see figure 9). These less-prominent fiber-forming jets can better be observed under different illumination conditions (the lighting utilized in the figure is to allow clear visualization of the fluid instabilities within the bowl) as shown later in the inset to figure 6 and in figure 7.

The jet formation process is visualized from a side view perspective in figure 5 where 55 kV is applied for the entire series of sequential camcorder images. A viewing slot was cut in the collector to laterally image the bowl and R6G used to tint the polymer fluid for better image contrast. The white LED light source is located below and outside the collector,

with the illumination direction 26° from the vertical. Here, the deformation when fluid is pulled over the bowl edge and upwards (approximately along the maximum electric field direction) is evident (2–6 s). During the first 17 s, various instabilities (both in and out of focus in the camera's fixed field of view) form, relax and regenerate; finally, at 18 s, a large deformation occurs near the camera focus. This instability then elongates, sharpens and produces a stream in the field of view at 25 s.

This unique visualization of the jet formation process from perspectives both above (figure 4) and to the side (figure 5) in this unconfined system highlights several important observations. First, in contrast with previous work [40] where thinning due to polymer solution droplets falling under gravity assisted the jet formation, here the electric field has sufficient amplitude to directly generate sharp fluid instabilities from which the stable, fiber-forming jets subsequently evolve. The jets appear to orient along the maximum local electric field direction at the bowl edge as illustrated in the expanded view of an isolated stable jet in figure 6. The linear region of the jet, viewed primarily from the side, where the polymer solution has been dyed with R6G for improved image contrast, does not take the shortest direct path to the grounded collector but is pointing at ∼29.2 ± 1.6° relative to horizontal, following the maximum electric field amplitude in the region as shown in the electric field simulations (figure 3). (This occurs both at the initiating as well as operating voltages, as the field distribution is the same in both conditions.)
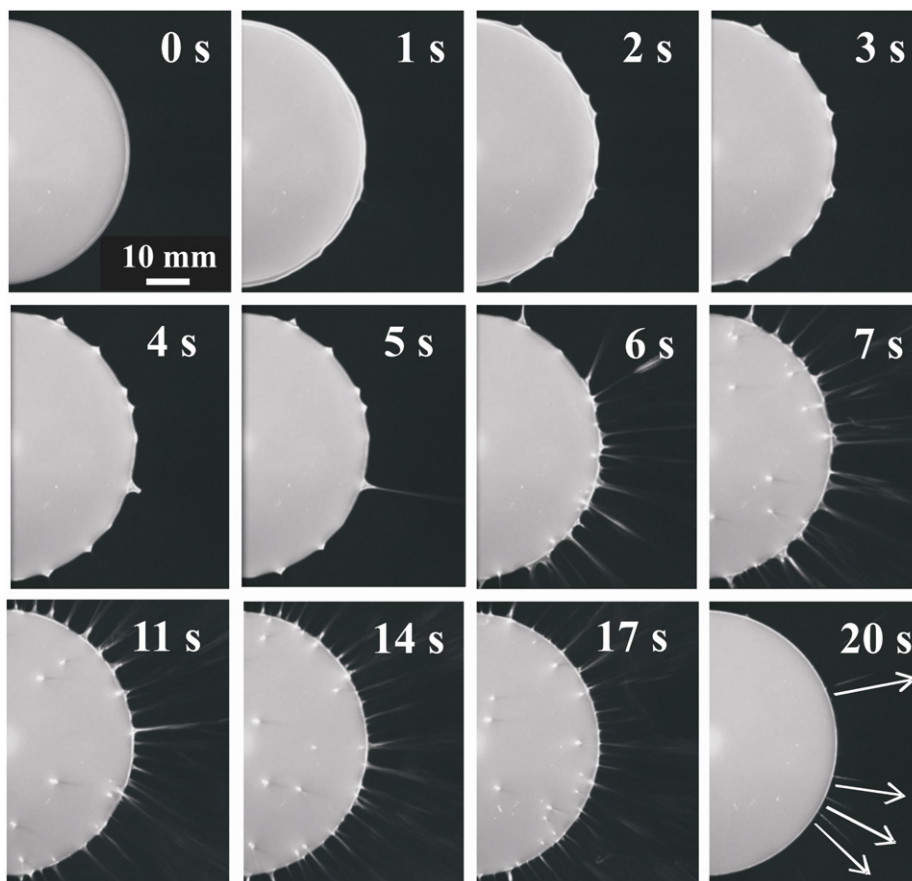
Figure 4. Sequential images of the jet initiation process occurring in bowl electrospinning as viewed from the top looking down. Multiple streaming jets are spontaneously formed throughout the initiation voltage interval (here 1–17 s) from (i) the top surface of the polymer solution and move radially outward or (ii) directly at the lip of the bowl. Stable jets (those most visible under this illumination scheme are highlighted by white arrows in the 20 s image) remain after the voltage is dropped to the steady state operating value of 16 kV.
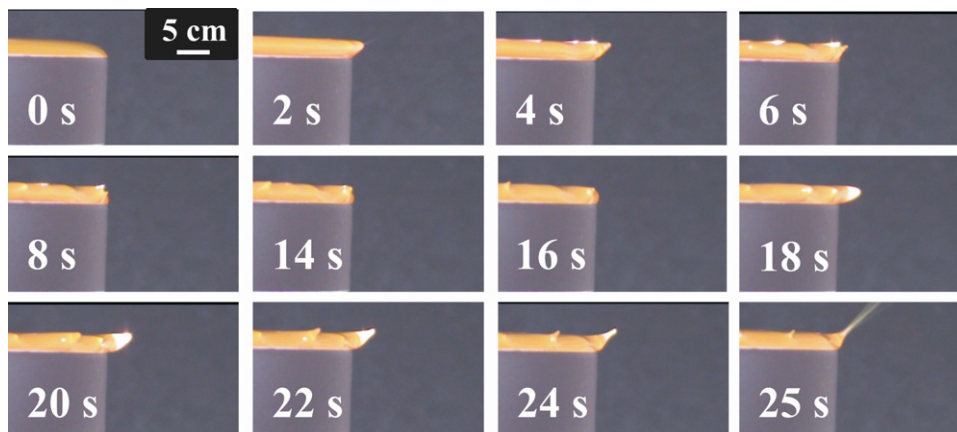
Figure 5. Sequential images (side view) from the camcorder video of the jet initiation process in bowl electrospinning. The bowl and cylindrical collector (not shown) are oriented concentrically. The voltage is turned on at 1 s and remains at the initiating amplitude (55 kV) throughout the sequence of images. The PEO solution is dyed with R6G for better viewing contrast. Multiple cones initiate from bowl edge throughout the initiation high voltage interval.

A second important point concerning jet initiation and exemplified by figures 4 and 5 is that there is initially a complex, seconds-long process of jet formation, splitting, relaxation and reorganization that ultimately produces the relatively evenly spaced stable jets (see figure 7). For most examples of the evolution of fluid instabilities from the interior of the bowl, initially a single jet spontaneously forms, followed rapidly by the production of multiple nearby jets, jet splitting and radial migration to the edge. In additional, many jets do form directly at the bowl's edge. We observed that if
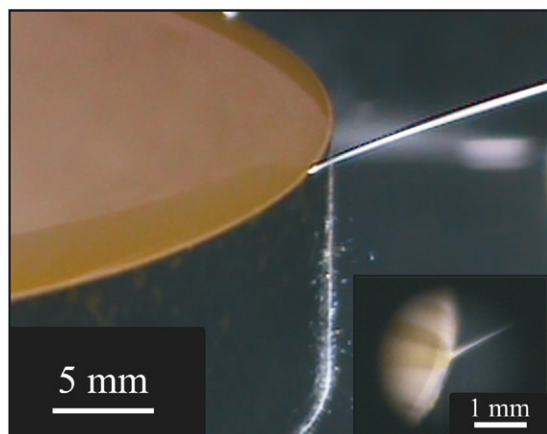
Figure 6. Image of an isolated stable jet electrospinning from the lip of the bowl, where the PEO solution is dyed with R6G for enhanced viewing contrast. Inset: a magnified image of the jet region using a monocular.


Figure 7. Digital SLR camera image of 37 stabilized jets electrospinning radially from the bowl edge as viewed from the top looking down. Linear and partial whipping regions are clearly visible. Note: the white features seen inside the bowl from this perspective are artifacts from bubbles in the polymer solution and the drain plug.

the high amplitude initiating voltage level is reduced to the lower operating voltage value shortly after the onset of jet formation, most of the streaming jets are extinguished and few stable jets will remain at the bowl edge. For the bowl size and the viscosity and conductivity of the PEO solution utilized, approximately ∼20 s of the high initiating voltage level is necessary to allow the jet formation process to mature, stabilize and fully populate the circumference of the bowl with useful jets before voltage reduction is implemented. After this stabilization period, when the voltage is reduced to the stable operating value, nearly all streaming jets smoothly transition to stable, fiber-forming spinning sites.

As noted earlier, a large electric field created via the high amplitude initiating voltage is necessary to spontaneously produce jets. At this required voltage level, the jets do not optimally electrospin and form fibers, but detrimentally transport fluid directly to the collector; however, when the voltage is reduced to the operating level, linear and whipping regions are formed and high quality fiber production occurs. For instance, figure 7 demonstrates ∼37 stable fiber-forming jets organized around the bowl edge. These jets spatially reside at the lip of the bowl as the polymer solution is fed in an unconfined manner from the volume of the bowl acting as a fluid reservoir; thus, the jets are typically stable for extended periods of time until the loss of solution causes the fluid level to drop below the bowl's edge. Under the stable operating condition, jet profiles from the bowl electrospinning process are quite similar to those generated by TNE except for the slight upward-angle jet orientation as noted above. As we previously reported, under optimal TNE conditions, the observed linear region corresponded to approximately 22% of the total working distance for a 5 μl min^{-1} feed rate which increased to 42% (at 15 μl min^{-1} feed rate) [40]. Here, the measured linear region is approximately 35% of the working distance, suggestive of an effective feed rate between the two values (see section 3.4).

In order to further demonstrate the broad applicability of this scale-up electrospinning technique, we also conducted preliminary experiments with an alternative polymer solution
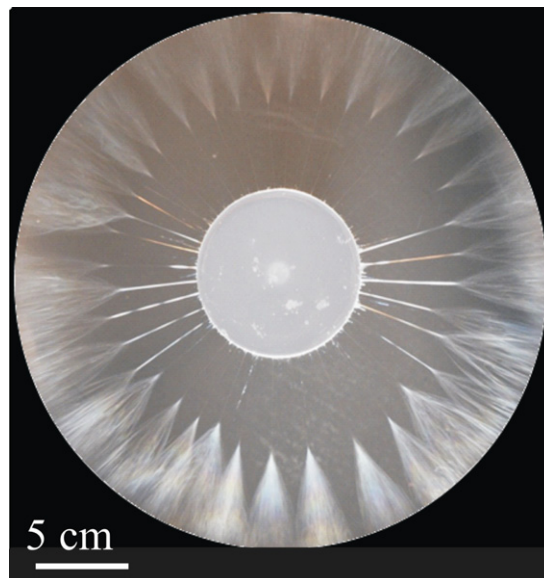
(12 wt% PCL) with significantly lower viscosity (170 cP) in a more volatile, non-aqueous solvent mixture (1:1 DCM:DMF, having individual vapor pressures of 47 and 0.4 kPa at 20 °C, respectively). For this polymer solution, no high amplitude initiating voltage was needed; jets both directly formed and stably produced fibers at a constant applied voltage of 30 kV. Decreasing the voltage below this value resulted in a rapid extinguishing of all existing jets and no new subsequent jet formation. Interestingly, at 30 kV, the fiber-forming jets were not as stable as in the PEO case, both continually extinguishing and re-initiating during the electrospinning process. In any electrospinning scheme (including TNE), such lack of stability will typically decrease nanofibrous mat quality as streaming or electrospraying events (which place the polymer solution directly onto the collector, degrading the existing fibers) often occur upon jet re-initiation. For a more concentrated PCL solution (16 wt%) having a larger viscosity value (3255 cP), the jet initiation process was similar to that observed for PEO; however, the higher volatility of the concentrated PCL solution detrimentally caused the rapid formation of thin PCL films on the fluid surface before jet stabilization could occur, thus preventing stable electrospinning and quality fiber formation. Future study will more precisely explore the parameters for optimal bowl electrospinning conditions for a range of polymers with different solution physical attributes (e.g. viscosity, volatility and conductivity) including the initiating (if needed) and stable operating regimes.

3.3. Fiber morphology

Table 1 summarizes the resultant fiber diameters for optimized PEO and PCL solutions electrospun in either the TNE or bowl geometry configurations. Figure 8 displays SEM images for
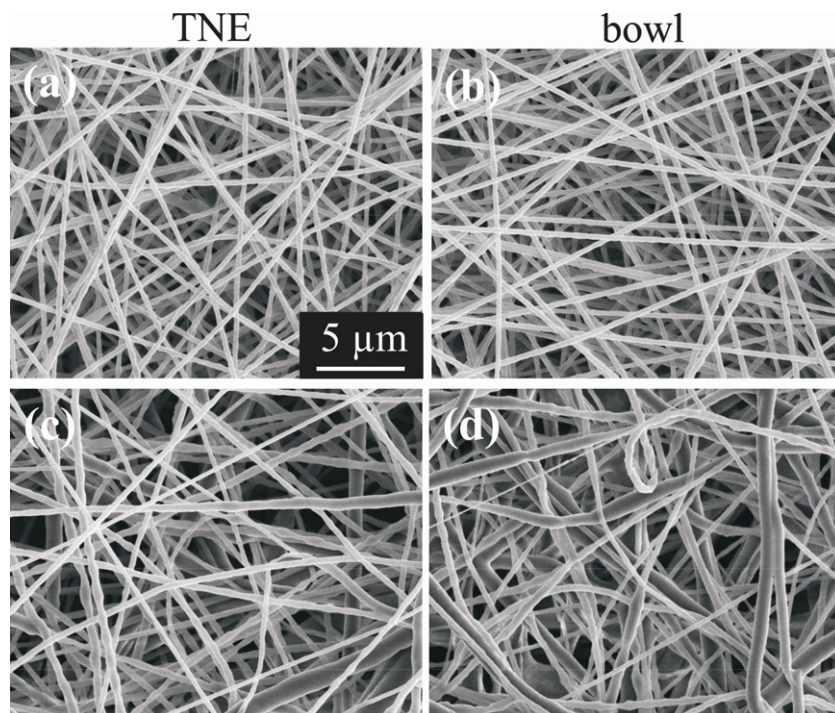
Figure 8. Comparing SEM images of nanofibrous mats composed of PEO (images (a) and (b)) and PCL (images (c) and (d)) fabricated under the two different configurations demonstrates that the bowl electrospinning technique (images (b) and (d)) produces similar quality nanofibers as those fabricated by TNE (images (a) and (c)).

Table 1. Comparison of fiber characteristics produced by TNE and bowl electrospinning for two different polymer systems. The working distance d is 15 cm for both configurations.

		PEO		PCL	
Set up	Applied voltage (kV)	Fiber diameter (nm)	Porosity (%)	Fiber diameter (nm)	Porosity (%)
TNE	11	262 ± 19	69.2 ± 1.6	374 ± 88	71.2 ± 1.5
Bowl	16	268 ± 25	67.6 ± 1.2	—	—
Bowl	30	—	—	344 ± 97	71.0 ± 1.1

the four cases. For both polymers, the mean fiber diameters, fiber distributions and mat porosity values produced from the two techniques are very similar, indicating that fibers of TNE-like quality can be readily produced via this scale-up approach. In the PEO case, where we have attempted some optimization of the parameters, the fiber quality is almost identical; however, even for preliminary, non-optimized studies of PCL (which has a significant heterogeneity of fiber diameters even for TNE), the quality of results are still similar. For both TNE and bowl electrospinning under the stable operating voltage, the spinnability of the fabricated mats is 100%.

3.4. 'Effective' feed rate

As previously reported [40], the electric field pattern of a sharp metal plate edge (see supplementary information, available at stacks.iop.org/Nano/22/345301/mmedia) is very comparable (in field magnitude and gradient) to that found near the jet-forming regions of a charged conducting needle (figure 3), but extended into two dimensions. In this present report, this edge is usefully curved around onto itself, forming an enclosed bowl

which can act as a polymer solution fluid reservoir while the electric field magnitude and gradient along a path normal from the bowl edge to the cylindrical collector remains very similar to that created in TNE (under the same working distance and applied voltage) from the needle to the flat collector. This electric field pattern is an important electrospinning parameter that governs the optimal nanofiber-forming process, affecting, for instance, jet formation as well as the length of the linear and whipping regions. Qualitatively matching the electric field pattern in bowl electrospinning to that exhibited in TNE provides for a similar set of forces which propel and elongate the jet as fibers are formed, likely accounting for the likeness in fiber quality between the dissimilar-appearing techniques. We note that, in contrast to the bowl geometry, many other scale-up approaches (for instance, a collection of closely spaced needle sources [44, 53, 54] or flat spinnerets [55, 56]) do not provide a similar electric field pattern as in TNE.

In TNE, optimal jet stability and nanofiber morphology are a result of the interplay of various processing parameters (for a given fixed polymer solution) such as feed rate, applied voltage and working distance, where the feed rate

Table 2. Comparison of mass throughput for single-batch bowl electrospinning of PEO for different times versus optimal TNE configuration. See figure 9 for a graph of the time evolution of stable bowl-spinning jets.

Spin time (min)	Mass throughput ($g\,h^{-1}$)	Average jets (#)	Mass throughput per jet ($g\,h^{-1}$)
20	0.684 ± 0.004	20.792 ± 5.227	0.0329 ± 0.0083
40	0.494 ± 0.001	18.232 ± 7.932	0.0271 ± 0.0118
90	0.265 ± 0.001	11.030 ± 9.314	0.0240 ± 0.0203
TNE	0.0167 ± 0.001	1	0.0167 ± 0.001

strongly influences fiber diameter. Within most confined electrospinning systems, the parameters listed above can be controlled independently; such is not the case for unconfined systems. In bowl electrospinning as an exemplary unconfined approach, the feed rate is essentially determined by the operating electric field (amplitude and spatial distribution), which must exquisitely balance the needs of jet stability and nanofiber formation. For too high an operating field, streaming (the uptake of too much fluid) occurs, resulting in larger diameter or poorly dried fibers, if they form at all (i.e. the condition which detrimentally occurs during the jet formation, high voltage interval); in contrast, an insufficiently robust operating electric field results in jet self-extinction (the uptake of too little fluid to maintain the jet cohesion or the inability to counteract fluid surface forces). Unlike TNE or other confined feed methods, polymer solution is not externally 'fed' at all, but rather must be 'pulled' from the fluid reservoir (here, the bowl itself) by the electric forces at a rate sufficient to form fibers of a certain diameter with a given speed of travel in the linear and whipping regions. Thus, the shape of the bowl at its edge and the amplitude of the applied voltage generate an 'effective' feed rate for the electrospinning process. Even with this important, significant alteration, the fiber quality produced from bowl electrospinning is almost identical to that from TNE.

3.5. Production rate

Table 2 summarizes the mass throughput for bowl electrospinning with PEO. The relative mass throughput per jet (which is thus directly proportional to this 'effective' feed rate) is summarized in the last column and enables comparison with that calculated from optimal TNE conditions. Thus, the bowl electrospinning feed rates (i.e. mass throughput) per jet are higher than, but within a factor of two, of the optimized feed rate for TNE. Consequently, by tuning the operating voltage for stable spinning in the bowl geometry, an effective feed rate is selected which is comparable to that in TNE. We conclude that since in bowl electrospinning both the effective feed rate and the pattern of electric field are very similar to that in TNE, consequently, the fiber formation process is also almost identical, allowing for the manufacture of high quality nanofibers but at a considerably increased throughput due to the many jets spaced along the edge of the bowl.

As dramatically shown in the digital SLR image (figure 7), one key advantage of bowl electrospinning is the circular symmetry and jet mobility on the fluid surface that enables
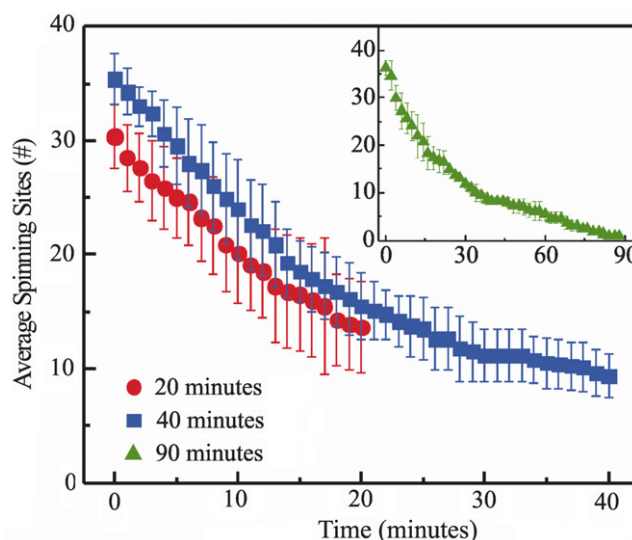
Figure 9. Time evolution of the number of stable jets for a single-batch spinning process for 20 min (red circles) and 40 min (blue squares), respectively. Each point is the calculated average and standard deviation from eight separate experiments. Upper inset: results from a single-batch spinning process for 90 min (green triangles) from three experiments.

the jets to facilely rearrange due to mutual electric repulsion, resulting in the population of the maximum number of spinning sites possible (for a particular fluid characteristics and applied electric field) approximately equally spaced over the circumference of the bowl. (Note: the jets are illuminated at an upward angle from below with two light sources (not shown) and an annulus-shaped mask blocks scattered light from the collector.) Within the unconfined feed method, the high voltage jet initiation interval (serving to rapidly overproduce numbers of potential stable jets), the fundamental jet mobility and subsequent reduction to a lower stable, operating voltage level act as natural feedback mechanisms to fully fill the available spinning sites. For PEO in figure 7, the initial number of jets after 1 min at the stable operating voltage was 37, corresponding to an average jet-to-jet minimum separation distance of 0.764 cm at the bowl's edge. Previously, in multiple-jet experiments [57], when needles were arranged in two-dimensional arrays with a jet-to-jet distance of 5 cm, the jets deflected from each other. In scale-up electrospinning when using an edge-plate geometry [40], if the fluid streams flowing down the plate which were supplying the multiple parallel spinning sites were located closer than 2.4 cm apart, the jetting process was intermittent and correspondingly reduced the fiber production rate. Here, in contrast, although the fiber forming sites are more closely spaced, stable electrospinning can occur for an extended time period. This is a consequence of the source–collector geometry: while the spinning sites at the bowl lip are more closely situated than in the parallel spinning configurations described above, the jets are radially oriented; thus jet-to-jet separation increases as one moves further away from the bowl. In these experiments a single dose of polymer solution (78 ml) was utilized, without a replenishing reservoir to actively maintain the fluid level in

the bowl during the spinning process. Because of the high mass throughput, the polymer solution continually depleted with time, dropping below the bowl edge and causing jets to extinguish; the remaining jets often rearranged to maintain a relatively equal site separation spacing until, at small jet numbers, the jet-to-jet repulsion was a minimal effect.

The evolution of the number of stable jets versus time (summarizing results from 19 individual experiments) is presented in figure 9. The loss of jets is due to two effects; first, at the stable operating voltage for high quality fiber formation, no new jets can spontaneously develop; therefore, extinguished spinning sites are not regenerated. Second, as the polymer solution level in the bowl drops due to the mass outflow in the fiber-forming jets, the spinning location has to follow the fluid and moves to a non-optimal location, where the balance between electric field characteristics (magnitude and gradient) and effective feed rate is not maintained. Thus, the decrease in the polymer solution fluid level in this single-batch process is the dominant underlying reason for the loss of jets. Nonetheless, despite lacking a replenishing reservoir, more than 10 jets were typically present after 40 min of spinning. As discussed above, the mass throughput per jet is within a factor of two of the mass throughput for TNE; thus the overall production rates scale proportionally as the number of jets multiplied by this effective feed rate enhancement factor. For this current size, if the initial number of stable jets were maintained, the system mass throughput would be ∼70 times that of TNE and with the same fiber quality. A current estimate (table 2) averages over 20 min of production, resulting in a 40-fold increase over TNE from an average of ∼21 jets; spinning for 40 min provides an enhancement of nearly 30 times from an average of ∼18 jets.

4. Conclusion

We have presented a novel, simple geometry for high throughput electrospinning that utilizes a bowl filled with polymer solution and a concentric cylindrical collector. Fibers produced from this edge electrospinning approach are almost identical in quality to those fabricated by TNE, with a demonstrated 40 times production rate increase. In this design, the electric field pattern is quite similar to that in single-needle electrospinning; as well, the feed rate per jet (which is determined by tuning the operating voltage) is also comparable to that from an optimized TNE experiment. Spinning was successful for two different polymer types with differing viscosity and solvent volatility. With the future engineering addition of a replenishing source to maintain the polymer solution level or refill the bowl during electrospinning, even greater increases in throughput are expected.

Acknowledgments

References

[1] Formhals A 1934 Process and apparatus for preparing artificial threads *US Patent Specification* 1,975,504
[2] Reneker D H and Chun I 1996 *Nanotechnology* **7** 216–23
[3] Shin Y M, Hohman M M, Brenner M P and Rutledge G C 2001 *Appl. Phys. Lett.* **78** 1149–51
[4] Shin Y M, Hohman M M, Brenner M P and Rutledge G C 2001 *Polymer* **42** 9955–67
[5] Lu X F, Wang C and Wei Y 2009 *Small* **5** 2349–70
[6] Burger C, Hsiao B S and Chu B 2006 *Annu. Rev. Mater. Res.* **36** 333–68
[7] Frenot A and Chronakis I S 2003 *Curr. Opin. Colloid Interface Sci.* **8** 64–75
[8] Huang Z M, Zhang Y Z, Kotaki M and Ramakrishna S 2003 *Compos. Sci. Technol.* **63** 2223–53
[9] Li D and Xia Y N 2004 *Adv. Mater.* **16** 1151–70
[10] Reneker D H, Yarin A L, Zussman E and Xu H 2007 Electrospinning of nanofibers from polymer solutions and melts *Advances in Applied Mechanics* vol 41 (San Diego, CA: Elsevier Academic) pp 43–195
[11] Subbiah T, Bhat G S, Tock R W, Pararneswaran S and Ramkumar S S 2005 *J. Appl. Polym. Sci.* **96** 557–69
[12] Barhate R S and Ramakrishna S 2007 *J. Membr. Sci.* **296** 1–8
[13] McCullen S D, Ramaswamy S, Clarke L I and Gorga R E 2009 *Wiley Interdisc. Rev. Nanomed. Nanobiotechnol.* **1** 369–90
[14] Barnes C P, Sell S A, Boland E D, Simpson D G and Bowlin G L 2007 *Adv. Drug Deliv. Rev.* **59** 1413–33
[15] Martins A, Araujo J V, Reis R L and Neves N M 2007 *Nanomedicine* **2** 929–42
[16] Murugan R and Ramakrishna S 2006 *Tissue Eng.* **12** 435–47
[17] Pham Q P, Sharma U and Mikos A G 2006 *Tissue Eng.* **12** 1197–211
[18] Vasita R and Katti D S 2006 *Int. J. Nanomed.* **1** 15–30
[19] Agarwal S, Wendorff J H and Greiner A 2008 *Polymer* **49** 5603–21
[20] Liang D, Hsiao B S and Chu B 2007 *Adv. Drug Deliv. Rev.* **59** 1392–412
[21] Xie J W, Li X R and Xia Y N 2008 *Macromol. Rapid Commun.* **29** 1775–92
[22] Cui W G, Zhou Y and Chang J 2010 *Sci. Technol. Adv. Mater.* **11** 11
[23] Goldberg M, Langer R and Jia X Q 2007 *J. Biomater. Sci. Polym. Edn* **18** 241–68
[24] Ignatious F, Sun L H, Lee C P and Baldoni J 2010 *Pharmaceut. Res.* **27** 576–88
[25] Sill T J and von Recum H A 2008 *Biomaterials* **29** 1989–2006
[26] Zahedi P, Rezaeian I, Ranaei-Siadat S O, Jafari S H and Supaphol P 2010 *Polym. Adv. Technol.* **21** 77–95
[27] Thavasi V, Singh G and Ramakrishna S 2008 *Energy Environ. Sci.* **1** 205–21
[28] Guo Q H, Zhou X P, Li X Y, Chen S L, Seema A, Greiner A and Hou H Q 2009 *J. Mater. Chem.* **19** 2810–6
[29] Hiralal P, Imaizumi S, Unalan H E, Matsumoto H, Minagawa M, Rouvala M, Tanioka A and Amaratunga G A J 2010 *ACS Nano* **4** 2730–4
[30] Im J S, Park S J and Lee Y S 2009 *Mater. Res. Bull.* **44** 1871–8
[31] Ji L W, Lin Z, Medford A J and Zhang X W 2009 *Carbon* **47** 3346–54
[32] Kim C 2005 *J. Power Sources* **142** 382–8
[33] Kim C, Yang K S, Kojima M, Yoshida K, Kim Y J, Kim Y A and Endo M 2006 *Adv. Funct. Mater.* **16** 2393–7
[34] Maity S, Downen L N, Bochinski J R and Clarke L I 2011 *Polymer* **52** 1674–85
[35] Greiner A and Wendorff J H 2007 *Angew. Chem. Int. Edn* **46** 5670–703
[36] Ramakrishna S, Fujihara K, Teo W E, Yong T, Ma Z W and Ramaseshan R 2006 *Mater. Today* **9** 40–50

[37] Dosunmu O O, Chase G G, Kataphinan W and Reneker D H 2006 *Nanotechnology* **17** 1123–7

[38] Varabhas J S, Chase G G and Reneker D H 2008 *Polymer* **49** 4226–9

[39] Zhou F L, Gong R H and Porat I 2009 *Polym. Int.* **58** 331–42

[40] Thoppey N M, Bochinski J R, Clarke L I and Gorga R E 2010 *Polymer* **51** 4928–36

[41] Ding B, Kimura E, Sato T, Fujita S and Shiratori S 2004 *Polymer* **45** 1895–902

[42] Tomaszewski W and Szadkowski M 2005 *Fibres Text. East. Eur.* **13** 22–6

[43] Varesano A, Rombaldoni F, Mazzuchetti G, Tonin C and Comotto R 2010 *Polym. Int.* **59** 1606–15

[44] Kumar A, Wei M, Barry C, Chen J and Mead J 2010 *Macromol. Mater. Eng.* **295** 701–8

[45] Jirsak O, Sysel P, Sanetrnik F, Hruza J and Chaloupek J 2010 *J. Nanomater.* **2010** 842831

[46] Yarin A L and Zussman E 2004 *Polymer* **45** 2977–80

[47] Lukas D, Sarkar A and Pokorny P 2008 *J. Appl. Phys.* **103** 7

[48] McCullen S D, Stano K L, Stevens D R, Roberts W A, Monteiro-Riviere N A, Clarke L I and Gorga R E 2007 *J. Appl. Polym. Sci.* **105** 1668–78

[49] McCullen S D, Stevens D R, Roberts W A, Clarke L I, Bernacki S H, Gorga R E and Loboa E G 2007 *Int. J. Nanomed.* **2** 253–63

[50] McCullen S D, Stevens D R, Roberts W A, Ojha S S, Clarke L I and Gorga R E 2007 *Macromolecules* **40** 997–1003

[51] Ojha S S, Stevens D R, Hoffman T J, Stano K, Klossner R, Scott M C, Krause W, Clarke L I and Gorga R E 2008 *Biomacromolecules* **9** 2523–9

[52] Ojha S S, Stevens D R, Stano K, Hoffman T, Clarke L I and Gorga R E 2008 *Macromolecules* **41** 2509–13

[53] Kong C S, Lee T H, Lee K H and Kim H S 2009 *J. Macromol. Sci.* B **48** 77–91

[54] Yang Y, Jia Z D, Li Q A, Hou L, Liu J N, Wang L M, Guan Z C and Zahn M 2010 *IEEE Trans. Dielectr. Electr. Insul.* **17** 1592–601

[55] Zhou F L, Gong R H and Porat I 2009 *Polym. Eng. Sci.* **49** 2475–81

[56] Zhou F L, Gong R H and Porat I 2010 *J. Appl. Polym. Sci.* **115** 2591–8

[57] Theron S A, Yarin A L, Zussman E and Kroll E 2005 *Polymer* **46** 2889–99